Design of Multilayer Dielectric Mirrors Optimized for Femtosecond Laser Pulses

Fredrik Bertilsson

Bachelor's thesis

Abstract

A general method for modelling reflection in a multilayer structure is developed. This is used to simulate how a Gaussian Ti:sapphire femtosecond pulse reflects off of a periodic SiO_2/TiO_2 dielectric stack at normal incidence. The method is based on a transfer matrix approach combined with the fast Fourier transform in MATLAB. Both a simple Bragg reflector and a linearly chirped mirror is investigated for three different pulse durations using mirrors with 5, 10, 20 and 40 layer pairs. It is demonstrated that a Bragg reflector is not suitable for reflecting a pulse shorter than 10 femtoseconds due to the limited reflectance bandwidth. The chirped mirror features a wider reflectance bandwidth but a reflected pulse exhibits strong group delay oscillations with wavelength, emanating from unwanted high-order dispersion in the mirror. Designs based on refined versions of this mirror type can however be used for reflection and dispersion compensation of pulses as short as 5 femtoseconds.

LUND UNIVERSITY

Division of Atomic Physics
Department of Physics

Supervised by Per Johnsson

May, 2015

Contents

List of abbreviations

as	attosecond
EM	electromagnetic
FFT	fast Fourier transform
fs	femtosecond
FWHM	full width at half maximum
GD	group delay
GDD	group delay dispersion
GVD	group velocity dispersion
HHG	high-order harmonic generation
IFFT	inverse fast Fourier transform
KLM	Kerr-lens mode locking
TE	transverse electric
TM	transverse magnetic
TMM	transfer matrix method

1 Introduction

1.1 Historical background

Since the first light of the laser in 1960, physicists have endeavoured to produce increasingly shorter pulses of laser light. The lasers of fundamental importance for today's research on ultrashort pulses operate with pulse durations on the order of femtoseconds (a femtosecond, 1 fs, is a millionth of a billionth of a second, 10^{-15} seconds). Such lasers have been around since the 1970s in the form of so called dye lasers, the laser type used in the experiments where femtosecond pulses were first produced [1]. However, dye lasers quickly proved to be far from ideal for short pulse generation: they deteriorate quickly, are weak in terms of output power and the highly toxic dye laser medium makes them complicated to handle.

Rapid progress was made when the much more versatile titanium-sapphire (commonly written Ti:sapphire) laser was introduced in the mid 1980s. This laser can be tuned to operate anywhere in a broad spectrum of wavelengths ranging from around 650 nm (1 nm = 10^{-9} m) to around 1100 nm. Such a broad bandwidth makes it highly suitable for short pulse generation. Most common to this day is operation at a wavelength of 800 nm (near infrared) where the Ti:sapphire lasing efficiency is at maximum. With techniques such as Kerr-lens mode locking (KLM), pulses of duation 5 fs (shorter than two optical cycles at 800 nm) have been achieved using Ti:sapphire lasers [2].

There are several areas of research where ultrashort pulses play an essential role. For example: to probe chemical reactions occuring on very short time scales, high temporal resolution is needed. One can make an analogy with photography: a high shutter speed is required if a moving object is to appear sharp in an image. Apart from probing fast chemical processes, a high-intensity femtosecond pulse can also stimulate certain reactions to occur. A pulse used in this manner is commonly referred to as a pump pulse. An experiment where the reaction is initiated by and then characterized with the same pulse is known as a pump-probe experiment. That is a very common approach in the field of femtochemistry, the study of very fast chemical processes.[1].

It is also possible to produce even shorter pulses of attosecond duration (1 as = 10^{-18} seconds) using femtosecond pulses. This happens in a process known as high-order harmonic generation (HHG), caused by the fact that the very high electric field of the laser pulse becomes comparable to the intra-atomic electric fields. Electrons in an atom targeted by the pulse can then escape the atomic potential and later recombine with the atom, thereby emitting attosecond pulses with wavelengths in the extreme ultraviolet range. Several pioneering experiments on HHG have been performed in Lund, both regarding pulse generation itself [4], [5] and characterization and applications of the generated pulses [6]. The pulses can be used to probe some of the fastest atomic and molecular phenomena occurring in nature [7].

[1] For a comprehensive summary of this field of research, see Ref. [3]

1.2 Purpose and motivation

A fundamental problem regarding ultrashort pulses is that they are inevitably distorted by ordinary optical components. After propagation through such components, the pulse will become severely broadened and might not even maintain its initial shape. Similar dispersive effects occur when such a short pulse traverses air (but not vacuum). At the end of an optical setup, it is thus likely that the pulse characteristics have become unsuitable for the intended application. The same problem can occur inside a laser in its resonating cavity.

The unwanted dispersion can be prevented or more or less effectively compensated for using more sophisticated optics. Since it may sometimes also be desirable to manipulate the initial pulse shape or duration, components can be tailored for such purposes as well. These components can for example be lenses, prism pairs[2], metallic filters or special multilayer mirrors known as dielectric mirrors. The latter have an additional advantage over ordinary mirrors since they can provide a much higher reflectance.

The purpose of this thesis is first and foremost to devise a simple and intuitive model which accurately describes the optical properties of a multilayer structure. More precisely, the aim is to study how well multilayer dielectric mirrors of varying design reflect a femtosecond pulse. How the shape of such a mirror shall be tailored to preserve the shape of an initially non-dispersed pulse and at the same time provide a very high reflectance is investigated. In this study, the materials of the constituting layers are chosen to be silicon dioxide (SiO_2, known as fused silica) and titanium dioxide (TiO_2) since they are commonly used in dielectric mirrors due to their suitable refractive indices. The mirror is modelled in MATLAB using a matrix approach together with the fast Fourier transform (FFT): the mirror acts as frequency domain filter. Each frequency component of the pulse is filtered separately since the refractive indices of SiO_2 and TiO_2 are frequency dependent. The spectral and temporal characteristics of the reflected pulse are then evaluated together with the mirror reflectance over a relevant frequency range. This is done for several different mirror designs and input pulse durations.

The thesis is organized as follows. In section 2 the theoretical background necessary to understand the results is treated. This starts with the mathematics of wave and pulse propagation followed by a discussion on the optical properties of dielectric media. The basis for the numerical method which the thesis is based on is then developed. The section concludes with a description of different dielectric mirror designs. In section 3 the method and analysis framework used is detailed. Section 4 is devoted to treating the results obtained in the simulations: the limits and prospects of each mirror design is discussed. The thesis is concluded in section 5 with an outlook reviewing current and future research on reflection and dispersion compensation of ultrashort pulses.

[2]Has been used for a Ti:sapphire laser [8].

2 Background

2.1 Mathematical description of ultrashort pulses

The material in this section is based on the treatment of the subject in sections 2.1, 2.2, 2.6, 5.6 and 22.1-3 in Ref. [9].

2.1.1 Fundamental properties of a wave

Light propagating in vacuum can be described as an electromagnetic (EM) wave with both the electric field **E** and the magnetic field **B** transverse to the direction of propagation. For propagation in the z-direction, the **E**-field amplitude $E(z,t)$ satisfies the *wave equation*:

$$\frac{\partial^2 E(z,t)}{\partial z^2} = \frac{1}{c_0^2}\frac{\partial^2 E(z,t)}{\partial t^2}, \tag{1}$$

where c_0 is the speed of light in vacuum and t is time. The **B**-field amplitude $B(z,t)$ satisfies an analogous equation. The behavior of the EM-wave can be completely described using either the electric or the magnetic field, since there is at all times a relation between E and B from Maxwell's equations: $E = B/c_0$. In this treatment, $E(z,t)$ is used. The most simple solution to the wave equation above is a sinusoidal wave of a single frequency ν:

$$E(z,t) = A\cos(\omega t + \varphi(z)), \tag{2}$$

where A is the (real) amplitude of the wave, $\omega = 2\pi\nu$ is the angular frequency and φ is a phase which translates the wave in the z-direction. The electric field amplitude is a real parameter, but it is conveniently described using a complex amplitude U written in terms of an exponential:

$$U(z,t) = Ae^{i(\omega t+\varphi(z))}. \tag{3}$$

$U(z,t)$ also satisfies the wave equation, with the same boundary conditions as $E(z,t)$. Using Euler's formula we get the following relation between real and complex amplitudes.

$$E(z,t) = \Re[U(z,t)] = \frac{1}{2}[U(z,t) + U^*(z,t)]. \tag{4}$$

It is now handy to separate U into its temporal and spatial parts, so that

$$U(z,t) = U(z)e^{i\omega t}, \tag{5}$$

where $U(z) = Ae^{i\varphi(z)}$ is the complex amplitude. We therefore get the phase from the argument of $U(z)$ and the amplitude from $|U(z)|$. If U is inserted into the wave equation it satisfies, we get the one-dimensional *Helmholtz equation*

$$\frac{\partial^2 U(z,t)}{\partial z^2} + k_z^2\, U(z,t) = 0, \tag{6}$$

where $k_z = \omega/c_0$ is the wave number: the spatial equivalent of the temporal angular frequency. This parameter is proportional to how many wavelengths $\lambda = c_0/\nu$ there is per unit length, and will be important later.

In many situations, the *intensity* $I(z,t)$ of a wave is a more important parameter than the electric field itself. It is proportional to the square of the E-field and a convenient definition is

$$I(z,t) \propto 2\langle E^2(z,t)\rangle, \tag{7}$$

where $\langle\cdots\rangle$ denotes time average. Inserting the expression for E in eq. (4) into the above definition, writing the exponentials of U and U^* in terms of sines and cosines and then time-averaging the surviving cosine term, one obtains that

$$I(z,t) \propto |U(z)|^2. \tag{8}$$

Therefore, the complex amplitude is of key interest. For a monochromatic (plane) wave its phase term looks like $\varphi(z) = -\mathbf{k}\cdot\mathbf{z} = -k_z z$. Using this, eq. (5) and Euler's formula, the full complex electric field can be written as

$$U(z,t) = A\,\mathrm{e}^{i(\omega t - k_z z)} = A\,\mathrm{e}^{i\omega(t-\frac{z}{c_0})}. \tag{9}$$

From this, both the spatial and temporal periodicity is clearly seen. It is also evident that for a given t, the overall phase of the wave depends on z/c_0. The velocity c_0 is therefore known as the *phase velocity*, which in this special case is the same as the propagation speed of the wave itself. If the wave propagates through a medium of refractive index n, its phase velocity is lowered by this factor: it immediately follows that λ must decrease with the same factor (so that k increases by n). The frequency thus stays the same regardless of n. The physical meaning of the refractive index will be elaborated on in section 2.2.

2.1.2 Temporal and spectral description

Wave equations on the form of eq. (1) are said to be *linear*. This means that if U_1 and U_2 are separate solutions, the sum of the solutions $U = U_1 + U_2$ is also a valid solution. Hence, one may construct any wave as a superposition of a (possibly infinite) number of individual plane waves. Since a plane wave is not localized in space it is not a very good description of real waves which are always localized in some way. Superimposing many plane waves of different wave numbers, it is possible to create a localized *wave packet*. Such a construct may accurately describe a wave only occupying a certain space at a given time, known as a *pulse*. It is very convenient to describe a pulse using the powerful Fourier transform approach. As implied above, a certain wave $E(t)$ at a certain position z may be written as a sum of plane waves, each of a unique amplitude $\hat{E}(\omega)$:

$$E(t) = \frac{1}{2\pi}\int_{-\infty}^{\infty} \hat{E}(\omega)e^{-i\omega t}d\omega. \tag{10}$$

Conversely, for a given $E(t)$ one may obtain its frequency components $\hat{E}(\omega)$:

$$\hat{E}(\omega) = \int_{-\infty}^{\infty} E(t)e^{i\omega t}dt, \tag{11}$$

known as the *spectrum*. Eq. (11) is the familiar Fourier transform. If $E(t)$ is a real function the negative frequency components are the complex conjugates of the positive ones. To avoid having to work with negative frequencies, one may just as before use a complex wave U. Then, $\hat{U}(\omega) = -\hat{U}(\omega)$: for $U(t)$ the Fourier components are symmetrically distributed around zero. Thus the integral in eq. (10) can instead be written from zero to infinity multiplied by a factor of two. Due to the linearity mentioned before, the real field $E(t)$ represented by the complex $U(t)$ can be obtained by an equation analogous to eq. (4).

The intensity is of a pulsed wave is given by the squared modulus of its complex amplitude $U(z,t)$. This can be motivated as follows. The intensity can be obtained as in eq. (7): insertion into this equation and subsequent rewriting leads to

$$I(z,t) \propto 2\langle E^2(z,t)\rangle = \frac{1}{2}\langle U^2(z,t)\rangle + \frac{1}{2}\langle U^{*2}(z,t)\rangle + \langle U(z,t)U^*(z,t)\rangle. \tag{12}$$

It can easily be shown that the two first terms oscillate at much higher frequency than the third term, which only contains differences of frequencies. Doing the time averaging over a sufficiently long time will then make the two first terms average out to zero so that only the last term remains, which is the desired result identical to that in eq. (8).

A sufficiently accurate model of the ultrashort pulses emitted by lasers like the Ti:sapphire laser is the pulsed plane wave. In the time domain, it is simply described by a plane wave of angular frequency ω_0 (the central or carrier frequency) with its amplitude modulated by some complex function C often called the *envelope*. At any given time and position in a material of (constant) refractive index n and $c = c_0/n$ it may thus be written as

$$U(z,t) = C\Big(t - \frac{z}{c}\Big)e^{i\omega_0(t-\frac{z}{c})}. \tag{13}$$

The temporal width of the envelope function is often described using the full width at half maximum (FWHM) of $I(z,t)$, here denoted τ_0. Spatially the pulse then occupies a FWHM of $c\tau_0$. Using the well known frequency shift property of the Fourier transform, $\hat{U}(z,\omega)$ at a given z becomes centered around ω_0 so that

$$\hat{U}(z,\omega) = \hat{C}(\omega - \omega_0)e^{-i\omega\frac{z}{c}}. \tag{14}$$

A general property is that a pulse of short duration (i.e. one whose $C(z,t)$ has a small τ_0) has a very broad spectrum; the opposite is true as well. If, as in the case of a pulsed plane wave, the phase is constant across all frequencies, the pulse is said to be *transform limited*. For an ultrashort pulse generated by a Ti:sapphire laser, C is at $z = 0$ temporally well described by a Gaussian envelope on the form in eq.(15) below. A Gaussian is very convenient, since its Fourier transform is also a Gaussian.

$$C(t) = e^{-\frac{\pi}{2}(\frac{t}{\tau})^2}. \tag{15}$$

With this definition of a Gaussian envelope, τ is not the FWHM of $I(t)$. Instead τ is the width of a square (top-hat) pulse which carries the same total energy as the entire Gaussian pulse. τ is somewhat smaller than τ_0 for a given pulse: we have that $\tau \approx 0.94\tau_0$. The product of this temporal duration and the spectral FWHM $\Delta\omega$ of C is constant: it is referred to as the *time-bandwidth product*. As a consequence, τ must increase if $\Delta\omega$ decreases and vice versa. This is sometimes called the *uncertainty relationship* between the time and frequency domains.

2.1.3 Dispersive media

Until now only propagation through a material with frequency independent refractive index has been considered. This is rarely the case for real materials: usually $n = n(\omega)$. Such a medium is said to be *dispersive*. A plane wave travelling through such a material is not affected by this since it is monochromatic. A pulse, which always has a spectral width > 0 will however be strongly affected. This is because the phase velocity is $c = c_0/n(\omega) = c(\omega)$, so the different frequency components in the pulse travel at different velocities. An initially transform limited pulse will thus, depending on whether n increases or decreases with frequency, eventually have low or high frequency components respectively in the leading part of the pulse. This is known as a *chirped* pulse.

For most materials n increases with ω in the visible and near-infrared parts of the spectrum. Such a medium exhibits *normal* dispersion, while in the other case the dispersion is said to be *anomalous*. The resulting pulse broadening can be understood from that the spectral phase is no longer constant: the pulse is then not transform limited and the time-bandwidth product $\tau\Delta\omega$ must increase. If one considers the temporal pulse shape at a fixed position, the frequency increases with time (positive chirp) for normally dispersive media and decreases (negative chirp) for media with anomalous dispersion. Figure 1 below demonstrates the difference between a chirped and transform limited pulse of duration $\tau = 10$ fs and central wavelength of 800 nm.

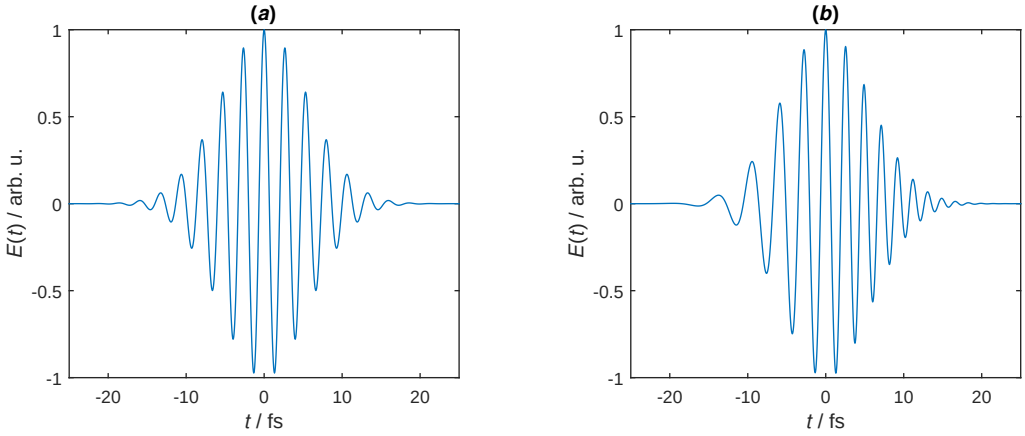

Figure 1: *A pulse with a Gaussian envelope of duration $\tau_0 = 10$ fs in the time domain. (a) Transform limited pulse. (b) Positively chirped pulse with chirp of $\approx$ +120 nm/fs.*

2.1.4 Parameters to describe pulse dispersion

Each component in a pulse starting at $z = 0$ and propagating in the positive z-direction will in a dispersive medium obtain a spectral phase

$$\varphi(\omega) = n(\omega)k(\omega)d, \tag{16}$$

after a distance $z = d$. Here $k(\omega) = \omega/c_0$ is the wave number in vacuum. To observe how $\varphi(\omega)$ has affected the pulse temporally at $z = d$, one may simply multiply each spectral component by $e^{-i\varphi(\omega)}$ and transform back into the time domain. We get:

$$U(z = d, t) = \frac{1}{\pi}\int_0^\infty \hat{U}(z = 0, \omega)e^{i(\omega t - \varphi(\omega))}d\omega. \tag{17}$$

It is now instructive to consider the case of a phase shift which varies sufficiently slowly with ω within the pulse. Then, $\varphi(\omega)$ can be Taylor expanded around the carrier frequency ω_0 keeping only the first term as below.

$$\varphi(\omega) \approx \varphi(\omega_0) + \frac{\partial\varphi}{\partial\omega}\Big|_{\omega=\omega_0}\big(\omega - \omega_0\big) = \varphi_0 + \varphi'(\omega - \omega_0). \tag{18}$$

Substituting this back into eq. (17), we obtain using $\delta = \omega - \omega_0$ that:

$$U(z = d, t) \approx \frac{e^{i(\omega_0 t - \varphi_0)}}{\pi}\int_0^\infty \hat{U}(z = 0, \delta)e^{i\delta(t-\varphi')}d\omega = \frac{e^{i(\omega_0 t - \varphi_0)}}{\pi}\int_{-\omega_0}^\infty \hat{U}(z = d, \delta)\, d\delta. \tag{19}$$

The exponential outside the integral corresponds to the carrier frequency wave, moving with its phase velocity $k_0 = \omega_0/c$. The integral describes the pulse envelope, which at the central frequency travels at the *group velocity* v_g. It can be easily obtained by dimensional analysis of the exponential inside the integral:

$$v_g(\omega_0) = \frac{d\omega}{d(kn(\omega))}\Big|_{\omega=\omega_0}. \tag{20}$$

Differentiating eq. (20) again, one obtains zero. What this means is that the pulse envelope is not distorted by the first term in the Taylor expansion in any way: it merely delays it by an amount $T_G = d/v_g$ known as *group delay* (GD). It can also be deduced that the group velocity is the same as the phase velocity at ω_0 if n is independent of ω, which is equivalent to including only one term in the expansion. However, if the pulse has a higher bandwidth (implying a shorter pulse), it will be necessary to include higher order terms. Such terms express a frequency dependent group delay and group velocity. The second term, for example, is called the *group delay dispersion* (GDD) and is written

$$\text{GDD} = \frac{d^2\varphi(\omega)}{d\omega^2}. \tag{21}$$

This term is responsible for the broadening and chirping effects that have been discussed in section 2.1.3. A related parameter is the *group velocity dispersion* (GVD) which is the GDD per unit length. One can continue and write the the third, fourth and higher order dispersion terms with their corresponding derivatives. These terms will alter the pulse shape in more complicated ways. For propagation in a material which has a given $n(\omega)$, high order terms become increasingly important with decreasing pulse duration.

2.2 On the refractive index

The refractive index of a material where the phase velocity is c for a given frequency is related to the electric permittivity $\epsilon = \epsilon_0\epsilon_r$ and magnetic permeability $\mu = \mu_0\mu_r$, with subscripts 0 and r indicating vacuum and relative permittivity/permeability. ϵ_r and μ_r are in turn dimensionless quantities related to the electric and magnetic *susceptibilities* $\chi_e = \epsilon_r - 1$ and $\chi_m = \mu_r - 1$. These determine how well a material is polarized/magnetized by the electric/magnetic components of the light wave as it propagates through the material. With the above relations, we can write

$$n = \frac{c_0}{c} = \sqrt{\frac{\epsilon\mu}{\epsilon_0\mu_0}} = \sqrt{\epsilon_r\mu_r}. \tag{22}$$

The materials of relevance in this thesis are *dielectrics*, which means that they are easily polarized by external electric fields but not very easily magnetized. Thus, $\mu \approx \mu_0$ is a reasonable approximation to make for such materials.

In the two sections above it has been assumed that no absorption occurs in the material: that the EM wave is not attenuated as it propagates. Absorption can easily be incorporated into the model by introducing a complex refractive index $n_c = n + i\alpha$ with α being the *attenuation coefficient*. This imaginary part adds a real term in the exponent of the complex wave $U(z,t) = e^{i\omega(t-z/c)}$, which thus becomes attenuated as z increases. However, for many dielectrics $\alpha \approx 0$ in the visible and near infrared region. For the small propagation distances of relevance in this thesis it is thus reasonable to neglect absorption and only include the real part n.

2.3 The Fresnel equations of transmission and reflection

Consider a plane EM-wave of wave vector $\mathbf{k}$ propagating in a dielectric of refractive index n_1 encountering a boundary to a dielectric of index n_2 at an angle θ_1 to the boundary normal. If there is no absorption, the wave will split into a refracted component $\mathbf{k'}$ and a reflected component $\mathbf{k''}$. Figure 2 on page 9 illustrates the situation. The ratio of the amplitudes depends on θ_1, n_2/n_1 and the incident wave polarization. If the polarization is such that the electric field is orthogonal to the plane spanned by $\mathbf{k}$ and $\mathbf{k''}$, it is said to be transverse electric (TE) or σ-polarized. The other case is transverse magnetic (TM) or π-polarization. An arbitrarily polarized wave is thus a linear combination of these polarization modes. Each mode is considered separately in the treatment that follows. The relationship between angles of incidence and refraction is determined by *Snell's law*:

$$n_1 \sin\theta_1 = n_2 \sin\theta_2. \tag{23}$$

We also have that $\theta_1 = \theta_3$ which is the law of reflection. These two results are independent of the polarization, however the amplitudes and phases of the refracted and reflected waves are not unless the angle of incidence is zero. Only considering the complex electric

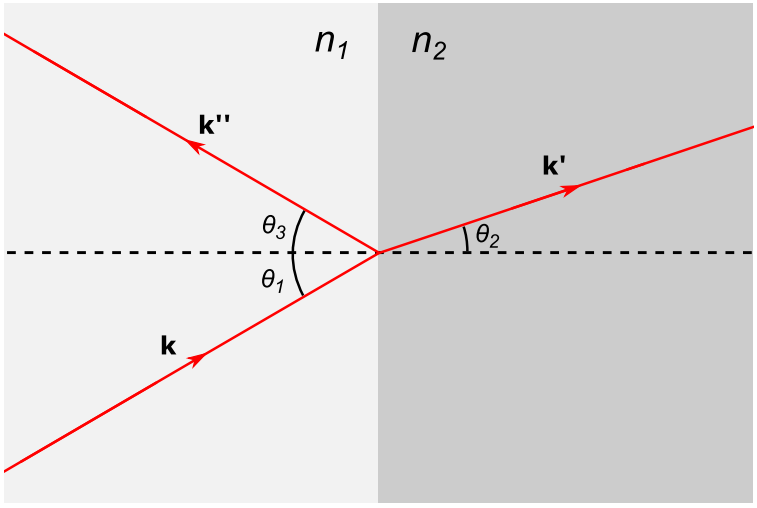

Figure 2: *Refraction and reflection of a plane wave with wave vector* **k** *incident on a boundary between two dielectrics of different refractive indices.* n_1 *is smaller than* n_2.

field U, we can write U' and U'' for refracted and reflected waves in terms of incident U using the complex *reflectance* r and *transmittance* t, with the only requirement being that $|r|$ and $|t|$ is ≤ 1 from energy conservation. r and t are complex and thus incorporate both amplitude and phase. For the two polarizations σ and π we get the following relations.

$$U'_\sigma = t_\sigma U_\sigma, \qquad U''_\sigma = r_\sigma U_\sigma. \tag{24}$$

$$U'_\pi = t_\pi U_\pi, \qquad U''_\pi = r_\pi U_\pi. \tag{25}$$

Now we only need to find r and t. They can be obtained by the boundary conditions provided by Maxwell's equations in materials: the parallel electric component and the transverse magnetic component must be continuous across the boundary regardless of the polarization. This combined with Snell's law gives the *Fresnel equations* below[3].

$$r_\sigma = \frac{n_1 \cos\theta_1 - n_2\sqrt{1-(n_1/n_2)^2\sin^2\theta_1}}{n_1 \cos\theta_1 + n_2\sqrt{1-(n_1/n_2)^2\sin^2\theta_1}}, \qquad t_\sigma = 1 + r_\sigma. \tag{26}$$

$$r_\pi = \frac{n_1 \sec\theta_1 - n_2\left(\sqrt{1-(n_1/n_2)^2\sin^2\theta_1}\right)^{-1}}{n_1 \sec\theta_1 + n_2\left(\sqrt{1-(n_1/n_2)^2\sin^2\theta_1}\right)^{-1}}, \qquad t_\pi = \frac{(1+r_\pi)\cos\theta_1}{\sqrt{1-(n_1/n_2)^2\sin^2\theta_1}}. \tag{27}$$

For normal incidence (i.e. $\theta_1 = 0$) the Fresnel equations reduce to the following for both polarizations:

$$r = \frac{n_1 - n_2}{n_1 + n_2}, \qquad t = 1 + r = \frac{2n_1}{n_1 + n_2}. \tag{28}$$

[3]For the full derivation, see pages 302-306 in Ref. [10]

If $n_1 < n_2$ as in figure 2, the reflection is said to be external. In this case r is real and negative. This means that the reflected wave experiences a phase shift of π, since $e^{i\pi} = -1$. Also, $\theta_1 > \theta_2$ if $\theta_1 \neq 0$. In the other case known as internal reflection there is no phase shift and $\theta_1 < \theta_2$ if $\theta_1 \neq 0$.

To get the intensity reflectance R representing the fraction of power in the incident wave that is reflected, one simply takes the modulus squared of r: $R = |r|^2$. Figure 3 illustrates how r and R depends on the ratio n_2/n_1 for external and internal reflection when $\theta_1 = 0$. As can be seen in figure 3b, the difference between the refractive indices should be as high as possible if the amount of reflection is to be maximized.

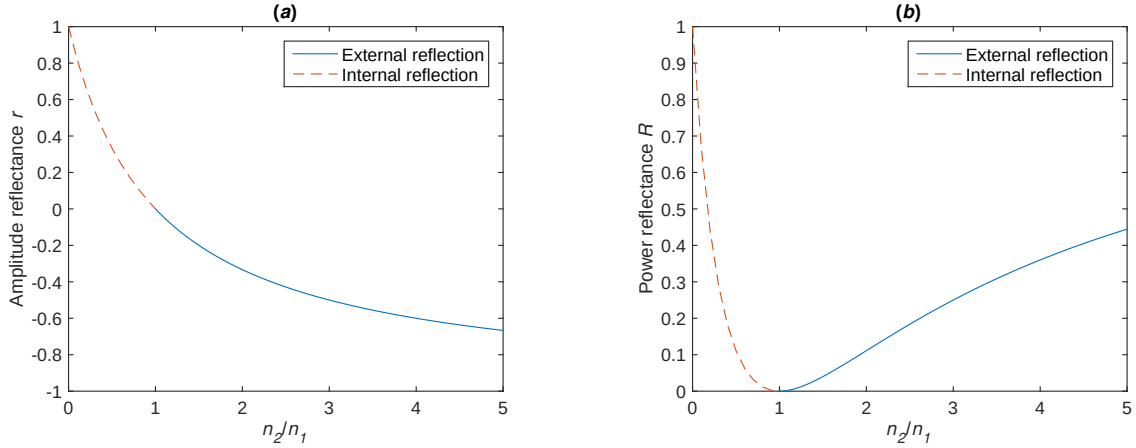

Figure 3: *Fresnel reflection coefficients for both external and internal reflection as function of n_2/n_1 at normal incidence. (a) Amplitude reflectance, r: note that it is negative for external reflection due to the phase shift of π. (b) Power reflectance, $|r|^2$.*

2.4 Scattering and transfer matrices

Most dielectrics suitable for mirrors have a refractive index below ≈ 3 in the visible and near-infrared range [11]. It is thus not sufficient with a single layer to obtain a high reflectance at normal incidence as is clearly demonstrated by figure 3. That is why multilayer dielectrics are used, as elaborated on in section 2.6. To theoretically describe pulse propagation through multilayer configurations, an analysis framework which incorporates both Fresnel reflection at the boundaries as well as dispersive propagation is required. Each frequency component in the pulse must be modelled to have obtained the correct phase and amplitude after reflection. Now, consider a single plane wave incident on a layered dielectric. It will separate into transmitted and reflected parts at each boundary, and those parts will continue to separate at other boundaries. The process results in a large number of interfering waves and it becomes very complex to keep track of them all. A pulse is a superposition of many different frequencies: modelling pulse propagation by simply using the Fresnel equations every time one of the frequency components hits a boundary is therefore even more complicated. Clearly, another approach is needed.

Due to the principle of superposition, all of the waves in a layer can be grouped together into a resulting pair of waves: one travelling in the positive direction (U_+) and one in the negative (U_-) as shown in figure 4. Thus we only get two terms for each layer (or four for each boundary), and so the complexity of the problem is greatly reduced. If the complex amplitude for each of the waves can be calculated at all points in the layer, we know how an incident plane wave propagates through and is scattered by the multilayer structure.

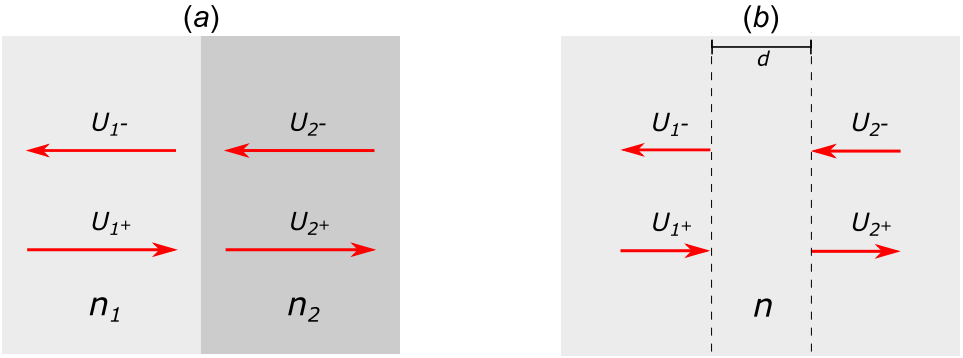

Figure 4: *An illustration of right and left-going waves in a dielectric. (a) Waves on each side of a boundary between two different dielectrics of refractive indices n_1 and n_2. (b) Waves on each side of a slab with refractive index n and width d.*

This approach makes it possible to describe the wave propagation with a matrix formalism. Consider one boundary in a multilayer structure, like the one in figure 4a. There are two complex waves on each side of the boundary: both incident (U_{1+}, U_{2-}) and outgoing (U_{1-}, U_{2+}) ones as illustrated. Due to the linearity of the wave equation the outgoing waves can be expressed in terms of the incident ones with a matrix S, defined as the *scattering matrix*:

$$\begin{pmatrix} U_{2+} \\ U_{1-} \end{pmatrix} = \mathrm{S} \begin{pmatrix} U_{1+} \\ U_{2-} \end{pmatrix} = \begin{pmatrix} t_{12} & r_{21} \\ r_{12} & t_{21} \end{pmatrix} \begin{pmatrix} U_{1+} \\ U_{2-} \end{pmatrix}. \tag{29}$$

The coefficients in the scattering matrix are thus the transmission and reflection coefficients given by the Fresnel equations: t_{12} is transmission from layer 1 to layer 2 for U_{1+} and so on. An S-matrix can also describe propagation through a medium as in figure 4b. Since the coefficients in S are complex they may incorporate the phase acquired during this propagation. For a medium of refractive index n and thickness d, the accumulated phase φ for a plane wave of vacuum wave number k is then $\varphi = nkd$. Therefore we get:

$$\begin{pmatrix} U_{2+} \\ U_{1-} \end{pmatrix} = \begin{pmatrix} e^{-i\varphi} & 0 \\ 0 & e^{-i\varphi} \end{pmatrix} \begin{pmatrix} U_{1+} \\ U_{2-} \end{pmatrix}. \tag{30}$$

The absence of reflection is thus clearly equivalent to the S-matrix being diagonal.

Another way of relating the wave amplitudes is to write the waves on the right side in terms of the ones on the left side. This can be done using the *transfer matrix* T:

$$\begin{pmatrix} U_{2+} \\ U_{2-} \end{pmatrix} = \mathrm{T} \begin{pmatrix} U_{1+} \\ U_{1-} \end{pmatrix} = \begin{pmatrix} \mathrm{T}_{11} & \mathrm{T}_{12} \\ \mathrm{T}_{21} & \mathrm{T}_{22} \end{pmatrix} \begin{pmatrix} U_{1+} \\ U_{1-} \end{pmatrix}. \tag{31}$$

The T-matrix coefficients are not as easily interpreted as the coefficients in the S-matrix. The two different approaches both completely describe the optical properties of a system, though, and relations between the coefficients of S and T may be derived since the two formalisms are equivalent. Performing the matrix multiplications, eqs. (29) and (31) can be written explicitly as

$$U_{2^+} = t_{12}U_{1^+} + r_{21}U_{2^-}, \qquad U_{1^-} = r_{12}U_{1^+} + t_{21}U_{2^-}. \tag{32}$$

$$U_{2^+} = \mathrm{T}_{11}U_{1^+} + \mathrm{T}_{12}U_{1^-}, \qquad U_{2^-} = \mathrm{T}_{21}U_{1^+} + \mathrm{T}_{22}U_{1^-}. \tag{33}$$

Solving for U_{2^-} in the second eq. (32) and inserting this expression in the first eq. (32), one obtains

$$U_{2^-} = \frac{1}{t_{21}}U_{1^-} - \frac{r_{12}}{t_{21}}U_{1^+}, \qquad U_{2^+} = \left(t_{12} - \frac{r_{12}r_{21}}{t_{21}}\right)U_{1^+} + \frac{r_{21}}{t_{21}}U_{2^-}. \tag{34}$$

By comparing these coefficients with those in eq. (33), it follows that

$$\mathrm{T} = \frac{1}{t_{21}}\begin{pmatrix} t_{12}t_{21} - r_{12}r_{21} & r_{21} \\ -r_{12} & 1 \end{pmatrix}. \tag{35}$$

With a similar approach, the converse relation can be obtained: the coefficients of the S-matrix expressed in terms of those in the T-matrix. The result is

$$\mathrm{S} = \frac{1}{\mathrm{T}_{22}}\begin{pmatrix} \mathrm{T}_{11}\mathrm{T}_{22} - \mathrm{T}_{12}\mathrm{T}_{21} & \mathrm{T}_{12} \\ -\mathrm{T}_{21} & 1 \end{pmatrix}. \tag{36}$$

To obtain the relations between transfer and scattering matrices describing propagation like in figure 4b, one can use a procedure identical to the one explictly written above. Figure 5 below illustrates the concepts of transfer and scattering matrices and how they relate complex wave amplitudes on the two sides of any optical component.

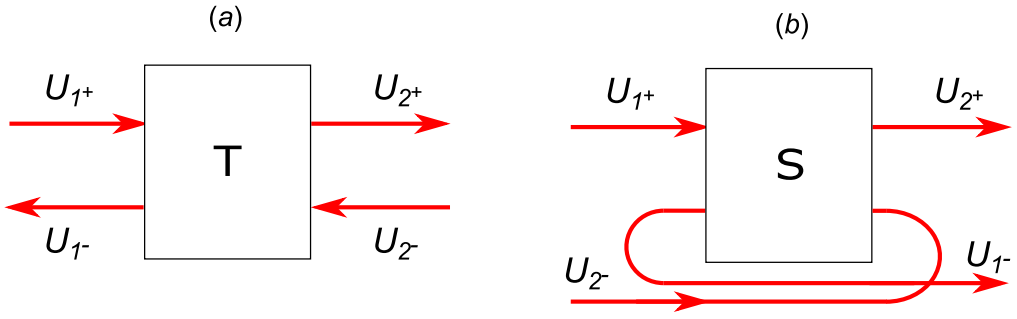

Figure 5: *How the two different matrix formulations relate complex wave amplitudes U, where the white boxes represent the optical system described by the matrices. (a) The transfer matrix connects waves on the left side with those on the right side. (b) The scattering matrix connects incoming waves with outgoing.*

2.5 The transfer matrix method

To analyze a multilayer structure, one can set up a scattering matrix to characterize every layer and boundary. The desired goal is of course to determine the transmission and reflection coefficients for the entire structure. To do this, all of the individual scattering matrices need to somehow be combined into a single one. Since a scattering matrix does not explicitly relate the left and right hand sides, it is not possible to simply multiply the individual matrices together to get the total matrix. It seems to be possible to combine them with the so called Redheffer star product [12], but this procedure is complicated and non-intuitive. On the other hand, multiple transfer matrices can be combined using ordinary matrix multiplication. To demonstrate this, consider the case of a boundary with vacuum to the left and a medium with refractive index n and thickness d on the right. There are then three pairs of right and left-going waves, U_L, U_R and U_d to the left, right and at distance d from the boundary respectively. The optical properties of the boundary and material are then determined by the matrices T_1 and T_2 so that

$$\begin{pmatrix} U_{R^+} \\ U_{R^-} \end{pmatrix} = \mathrm{T}_1 \begin{pmatrix} U_{L^+} \\ U_{L^-} \end{pmatrix}, \qquad \begin{pmatrix} U_{d^+} \\ U_{d^-} \end{pmatrix} = \mathrm{T}_2 \begin{pmatrix} U_{R^+} \\ U_{R^-} \end{pmatrix}. \tag{37}$$

By inserting the expression for U_R from the first equation into the second, we obtain

$$\begin{pmatrix} U_{d^+} \\ U_{d^-} \end{pmatrix} = \mathrm{T}_2\mathrm{T}_1 \begin{pmatrix} U_{L^+} \\ U_{L^-} \end{pmatrix}. \tag{38}$$

Thus the matrix $T_{tot} = T_2T_1$ is a complete description of the composite optical system. It is easy to generalize this result to apply for N transfer matrices. In that case we get

$$\begin{pmatrix} U_{N^+} \\ U_{N^-} \end{pmatrix} = \mathrm{T}_N\mathrm{T}_{N-1}\cdots\mathrm{T}_2\mathrm{T}_1 \begin{pmatrix} U_{1^+} \\ U_{1^-} \end{pmatrix}. \tag{39}$$

Putting everything together one can conclude that if d and n of every layer is known, there is a completely general procedure to find the total Fresnel coefficients. Start by determining the Fresnel coefficients for every boundary and the phase φ for the propagation between the boundaries. This is equivalent to determining the S-matrices. Then use eq. (35) to convert them into T-matrices in order to exploit the multiplicative property implied in eq. (39). After having carried out the multiplication, use eq. (36) to convert the resulting T-matrix to the S-matrix for the entire structure. The optical properties of the multilayer are thereby obtained. The procedure outlined above is in this thesis referred to as the *transfer matrix method* (TMM) and can be used to model propagation through any kind of multilayer optics.

2.6 Dielectric mirrors

If a mirror is to reflect an ultrashort pulse well, its reflectance must of course be very high over the entire bandwidth of the pulse. For a pulse with a FWHM of 10 fs in the time

domain and carrier wavelength $\lambda_0 = 800$ nm, the bandwidth FWHM is almost 200 nm. In order for most of the pulse to be reflected, the region of high reflectance in frequency space must thus be much wider than this. One can obtain a rather high reflectance across such a bandwidth using a mirror in the form of a thin sheet of metal such as silver or gold. This is the common type of mirror used in almost any type of optical setup. Another advantage with such metallic mirrors is that since there is no propagation through a dispersive material, the pulse shape remains essentially the same after reflection. However, the reflectance is not high enough for many ultrashort pulse applications: it is hard to achieve a power reflection coefficient larger than 99 % [13]. A pulse of short duration means a very high peak intensity, and the small fraction of absorbed light may very well be enough to significantly heat the thin metallic layer. The damage caused by this can either change the optical properties of the mirror in an undesired way or even completely destroy it. Other mirror designs must thus be considered for the short, high-intensity pulses used in modern femtosecond Ti:sapphire laser systems.

2.6.1 The Bragg reflector

A reflectance much higher than 99 % can be obtained using a stack of dielectrics with layers of alternating refractive index. The low index layers l usually have $n_l \approx 1.5$ while the high index layers h have $n_h \approx 2.5 - 3$: common materials are silicon dioxide (SiO_2) and titanium dioxide (TiO_2) respectively. At the value of n_h/n_l for these materials, the Fresnel reflectance at each boundary is not very high as demonstrated in figure 3. The reflections at all boundaries will however add up with the result being that the total reflectance grows quickly with the number of layers in the stack.

The layer thickness d is an important parameter since it determines how much phase a propagating wave acquires. A dielectric mirror of the kind discussed above will not work as well if the reflected waves are out of phase with each other and interfere destructively. Maximum reflection will occur when the optical thickness nd is equal to a quarter of the light wavelength. In this case all reflected waves will interfere constructively which can be understood as follows. If the reflection occurs from a low-index medium the phase shift is π. The light incident on this boundary has aquired a phase of $\pi/2$ from propagation before reflection, and acquires this same phase after reflection as well: it adds up to a phase of 2π, exactly one wavelength. Light reflected from the previous and next boundary is internally reflected and is thus not phase shifted in the reflection process. These three reflected waves will then all have the desired phase difference of an integer number of 2π and by extension this is true for all reflected waves. Such a mirror is called a *Bragg reflector* since the condition for constructive interference is similar to the famous Bragg's law describing the scattering of X-rays off of a crystal lattice. The temporal effects such a mirror has on an ultrashort pulse are extensively studied in this thesis.

2.6.2 More complex designs

A short pulse is very sensitive to the group delay variations induced by propagation through even a short distance in a dispersive dielectric. It should however be possible to

modify the structure of a thin Bragg reflector slightly so that the reflected pulse exhibits a certain GD variation profile. Therefore a dielectric mirror might be used to compensate for GD variations in the incident pulse. The most basic way to do this is to vary the optical thickness with the layer depth. Thereby the different spectral constituents in the pulse are maximally reflected at different mirror depths, which clearly introduces a GDD. Such mirror designs are usually referred to as *chirped* in analogy with the previously discussed concept of frequency chirp. It is not trivial to determine just how the mirror shall be chirped for a certain GD variation profile to be obtained: the problem is often solved using numerical optimization instead of being deduced by principle.

2.6.3 Manufacturing techniques

Since the layers must be very thin (on the order of hundreds of nanometers for visible light) for the Bragg condition to be satisfied it is not so easy to actually fabricate a dielectric mirror. The thickness of only some thousand atoms per layer also makes the mirror prone to deposition irregularities at the layer boundaries. Such manufacturing errors may induce significant undesired effects like diffuse reflection, resulting in a spatial spread of the pulse. It is therefore crucial to use a deposition method with very high precision. Various procedures are available: some commonly used ones are electron beam deposition, ion-assisted deposition and ion beam sputtering [14]. Via such procedures, multilayer optics can be produced whose reflection characteristics agree well with theoretical results.

3 Method

3.1 General description

The basic idea behind the analysis framework used in this thesis is to combine the TMM with the FFT in the programming language MATLAB. In the version of the TMM described in section 2.5 it is assumed that the input wave is monochromatic. This approach can also be used to model a pulse since a pulse is a linear combination of plane waves. However, every frequency component has to be sent through an individual TMM-routine since the mirror materials are dispersive. The entire procedure from input pulse to reflected pulse is described below.

The complex electric field amplitude $U_0(t)$ of the input pulse is defined and discretized in temporal space in MATLAB. It is then Fourier transformed using FFT into frequency space so that $U_0(\omega)$ is obtained. Frequency components that have an intensity $|U_0(\omega)|^2$ larger than a certain value are then selected: these are the plane waves for which the TMM shall be applied. This selection is done since components of very low amplitude barely affects the shape of the pulse, and so these can be neglected. Now the refractive indices $n(\omega)$ for the mirror materials must to be obtained. They are needed since they are crucial for determining the reflection and propagation S-matrices: every frequency component must acquire the correct reflection coefficients and propagation phase $\varphi = nk_0d$. At this stage the mirror structure must be decided upon: the amount of layers and the thickness

d of every layer is chosen. The Fresnel equations are used to find the coefficients of all boundary S-matrices. When they are determined, the TMM is applied for every selected frequency by for-looping through all frequencies. The desired complex reflectance $r_{12} = r(\omega)$ is obtained from the total T-matrix: $r(\omega) = -\mathrm{T}_{21}(\omega)/\mathrm{T}_{22}(\omega)$.

Now it is known how each complex wave constituting the selected input pulse is affected by the reflection. This is equivalent to knowing how the pulse itself is affected. We get the reflected pulse $U(\omega)$ in frequency domain by simple element-wise multiplication: $U(\omega) = r(\omega)U_0(\omega)$. The mirror thus acts as a frequency domain filter. To evaluate the temporal properties of the reflected pulse the inverse FFT (IFFT) in MATLAB is used to obtain $U(t)$ from $U(\omega)$.

3.2 The input pulse

Let the pulse be incident from the left onto the mirror at $z = 0$ and assume that the propagation occurs along the z-axis only. This means that the angle of incidence is zero and that r_{12} is the relevant reflection coefficient. Only the temporal shape of the reflected pulse at this same point is of interest. Thus it is not necessary to include the z-dependence in the expression for the input pulse. As implied in section 2.1.2 the input pulse will be assumed to be Gaussian, and will at $z = 0$ be on the form

$$U_0(t) = e^{-\frac{\pi}{2}(\frac{t}{\tau})^2} e^{i\omega_0 t}, \tag{40}$$

where ω_0 corresponds to the central wavelength of 800 nm for a Ti:sapphire laser. Figure 6 shows the temporal and spectral intensities of the three transform limited input pulses used in the simulations: pulses of top-hat durations $\tau = 5$, 10 and 20 femtoseconds. It is clear that a higher pulse duration means a narrower bandwidth and vice versa.

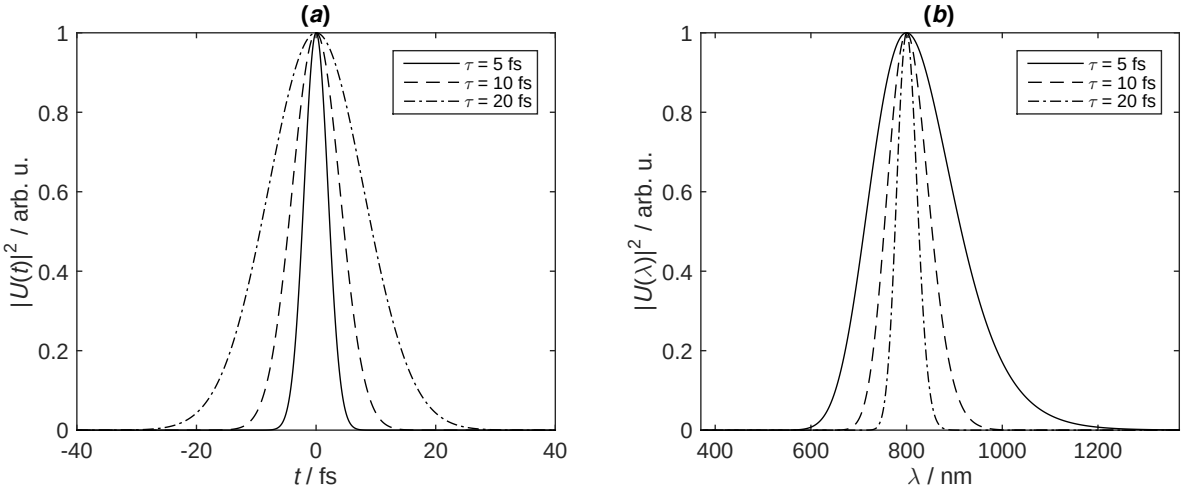

Figure 6: *The three input pulses in both the time and frequency domain. (a) Temporal intensity $|U_0(t)|^2$. (b) Spectral intensity $|U_0(\lambda)|^2$. The non-Gaussian shapes are due to that $|U_0(\omega)|^2$ is Gaussian, and therefore intensity as function of λ is not.*

3.3 Refractive indices and mirror designs

As demonstrated by figure 6 the range of wavelengths selected to be filtered by the TMM must be at least 600-1300 nm for the shortest pulse. Therefore the dispersion curves $n(\lambda)$ for SiO_2 and TiO_2 should reliably cover this range of wavelengths. Refractive indices as function of wavelength were obtained as data files[4] from Refs. [17] and [18] for SiO_2 and TiO_2 respectively. To be certain to cover as much of the pulse as possible, data ranging from 375 to 1370 nm was used for both materials. To match a value of n to every λ in the chosen wavelength range, least square-fits to 10-degree polynomials[5] were made to the data points obtained from the .txt-files. Figure 7 shows the data points along with the fitted curves for both materials. As can be seen, the curves accurately describe the material dispersion across the chosen filtering wavelength range of 375-1370 nm.

For each mirror type, several different designs were modelled. First and foremost the number of layer pairs of SiO_2/TiO_2 was varied, since it is the most obvious parameter that should affect the features of the reflected pulse. It was also tested if it mattered whether the outermost layer was TiO_2 or SiO_2. At all times it was assumed that there was vacuum (with $n(\lambda) = 1$) outside the mirror. With the simple Bragg mirror 5, 10, 20 and 40 layer pairs were tested for each input pulse. The thickness of the layers are obtained from the Bragg condition and is about 138 and 90 nm for SiO_2 and TiO_2-layers respectively.

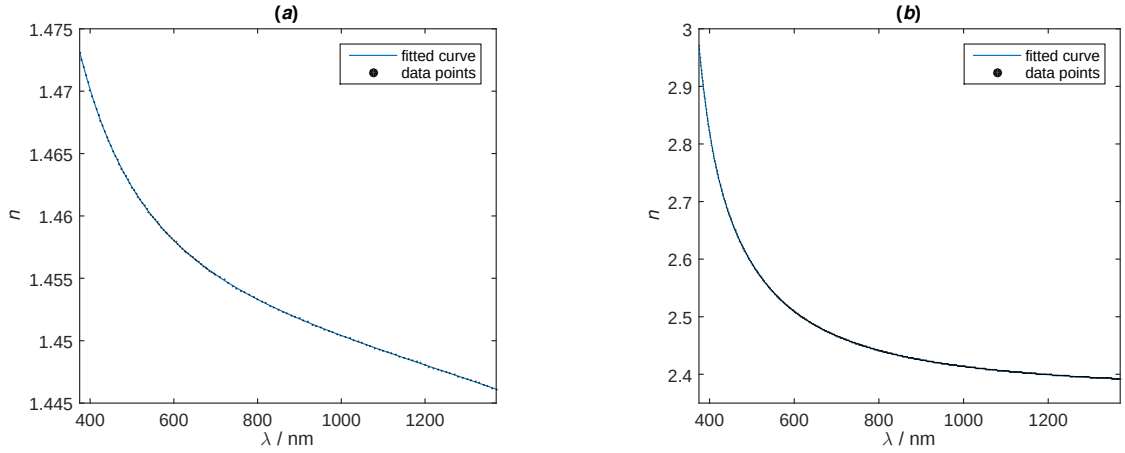

Figure 7: *Refractive index data and fit for the two materials constituting the mirrors. (a) Silicon dioxide (fused silica), SiO_2. (b) Titanium dioxide, TiO_2.*

A linearly chirped mirror structure was also modelled for the three different pulses. Linear chirp means that the Bragg wavelength varies uniformly with the depth in the mirror. This type of chirp was investigated for the same amount of layer pairs as for the Bragg mirrors, since one can then directly compare the similarities and differences between the two designs.

[4] These are in turn extrapolations of data from actual measurements in Refs. [15] and [16] respectively.

[5] This is the highest order supported by MATLABs "basic fitting" and was deemed satisfactory as supported by the very good fits shown in figure 7.

3.4 Evaluating the results

Several parameters are employed to describe the reflected pulse. Two of these measures reflectance. They are the mirror reflectivity $R(\lambda) = |r(\lambda)|^2$ which is plotted, and the integrated power reflectance R_{tot} for the pulse given by

$$R_{tot} = \frac{\int_{\omega_{min}}^{\omega_{max}} I(\omega) d\omega}{\int_{\omega_{min}}^{\omega_{max}} I_0(\omega) d\omega}, \tag{41}$$

where ω_{min} and ω_{max} are the frequencies delimiting the filtering range. R_{tot} is calculated for the different designs, as is the ratio of temporal peak intensities $R_{max} = I(t)_{max} / I_0(t)_{max}$.

The value of R_{max} indicates how much the pulse is smeared out in the time domain. Several other parameters describe how the temporal shape of the pulse is affected by the mirror. Among them is the accumulated phase $\varphi(\lambda)$, which determines how much the different frequencies in the pulse have been delayed. More specifically it determines the GD and the GDD given by the first and second derivative of $\varphi(\omega)$ respectively. The GD is plotted across the range of filtered wavelengths for some selected mirror designs. Also plotted is the electric field $E(t) = \Re[U(t)]$ for these designs which provides a direct measure of what the pulse looks like in the time domain after reflection.

4 Results and discussion

4.1 The Bragg mirror

Reflection properties of the eight different Bragg mirrors and the three input pulses that were modelled are summarized in tables 1 and 2 on the format $[R_{tot} / R_{max}]$. In the mirror types represented by table 1 both the substrate and outermost layer was SiO_2 while it was TiO_2 for the mirror types in table 2. It is clear that the longer pulses are reflected

Table 1: *Power reflectance coefficient R_{tot} / ratio of peak intensities R_{max} for the different input pulses and mirror designs with SiO_2 as substrate and outermost layer.*

Number of layer pairs	Pulse duration τ / fs		
	5	10	20
5	0.90244 / 0.70772	0.96230 / 0.94685	0.96697 / 0.96569
10	0.92948 / 0.70789	0.99870 / 0.97432	0.99980 / 0.99974
20	0.92963 / 0.70789	0.99899 / 0.97433	1.0000 / 0.99998
40	0.92968 / 0.70798	0.99899 / 0.97437	1.0000 / 0.99998

better than shorter ones regardless of the number of layers or mirror type used. Also, R_{tot} and R_{max} both increase rapidly with the layer number for $\tau = 10$ and 20 fs but not as rapidly for the shortest pulse. The rate of increase also decreases at high layer numbers: the difference is generally larger going from 5 to 10 layer pairs than going from 20 to 40.

Table 2: *Power reflectance coefficient R_{tot} / ratio of peak intensities R_{max} for the different input pulses and mirror designs with TiO_2 as substrate and outermost layer.*

Number of layer pairs	Pulse duration τ / fs 5	10	20
5	0.92203 / 0.72741	0.98738 / 0.96752	0.99035 / 0.98964
10	0.92972 / 0.72741	0.99890 / 0.97339	0.99994 / 0.99988
20	0.92977 / 0.72741	0.99899 / 0.97339	1.0000 / 0.99995
40	0.92974 / 0.72732	0.99899 / 0.97335	1.0000 / 0.99995

This indicates that most of the reflected frequencies do not penetrate much past the 20th layer pair. Having the high index material as substrate and outermost layer seems slightly beneficial over the other configuration in nearly all cases: it is thus chosen to be the mirror type of focus in the analysis that follows.

Apparently the 5 fs pulse is reflected much worse than the longer pulses for every mirror configuration. This implies that a simple Bragg mirror is not very suitable for pulses of such short duration: R_{tot} is rather low and R_{max} even lower, indicating a smearing of the pulse in the time domain. To identify the reason for this it is instructive to consider $R(\lambda)$, shown in figure 8 for the TiO_2-substrate mirrors, and $E(t)$ as well as $GD(\lambda)$, shown in figure 9 for the same mirror type with 20 layer pairs.

The mirror reflectance evidently increases with the number of layers inside a band of wavelengths around the Bragg wavelength: this band is henceforth referred to as the "stop band". Even for only 5 layer pairs, most wavelengths of light between 750 and 850 nm are well reflected ($R \approx 0.99$). For 10 layer pairs this has increased to a reflectance of about 99.9 %, easily surpassing that of a good metallic mirror. The stop band is also somewhat widened. Further increasing the number of layer pairs results in an extremely high reflectance between 700 and 950 nm. The stop band does not seem to widen much beyond this wavelength range, however. Outside the band the reflectance does not rise further by increasing the number of layers: this only raises the number of peaks where the reflectance is semi-high ($0.2 \leq R \leq 0.9$). Figure 8b is similar to figure 7.1-11 in Ref. [9] where a structure with 10 layer pairs of refractive indices of 1.5/3.5 is used. This suggests that the general features of the results shown in figure 8 are what one could expect from any Bragg mirror. It is further supported by a striking resemblance of figure 8c with figure 3.5 a) in Ref. [19] where a 20 layer SiO_2/TiO_2 mirror structure is modelled.

Comparing figure 8 with the input pulses in figure 6, it is easy to understand why the reflectance decreases with pulse duration. The 20 fs pulse has a bandwidth clearly within the stop band and is consequently very well reflected. For the 10 fs pulse the situation is somewhat worse with a bandwidth slightly larger than that of the stop band, which explains the smaller values of R_{tot} in tables 1 and 2. The bandwidth of the 5 fs pulse is wider than the stop band by a substantial amount and so a lot of frequency components in the pulse are not very well reflected. This is true regardless of the number of layers.

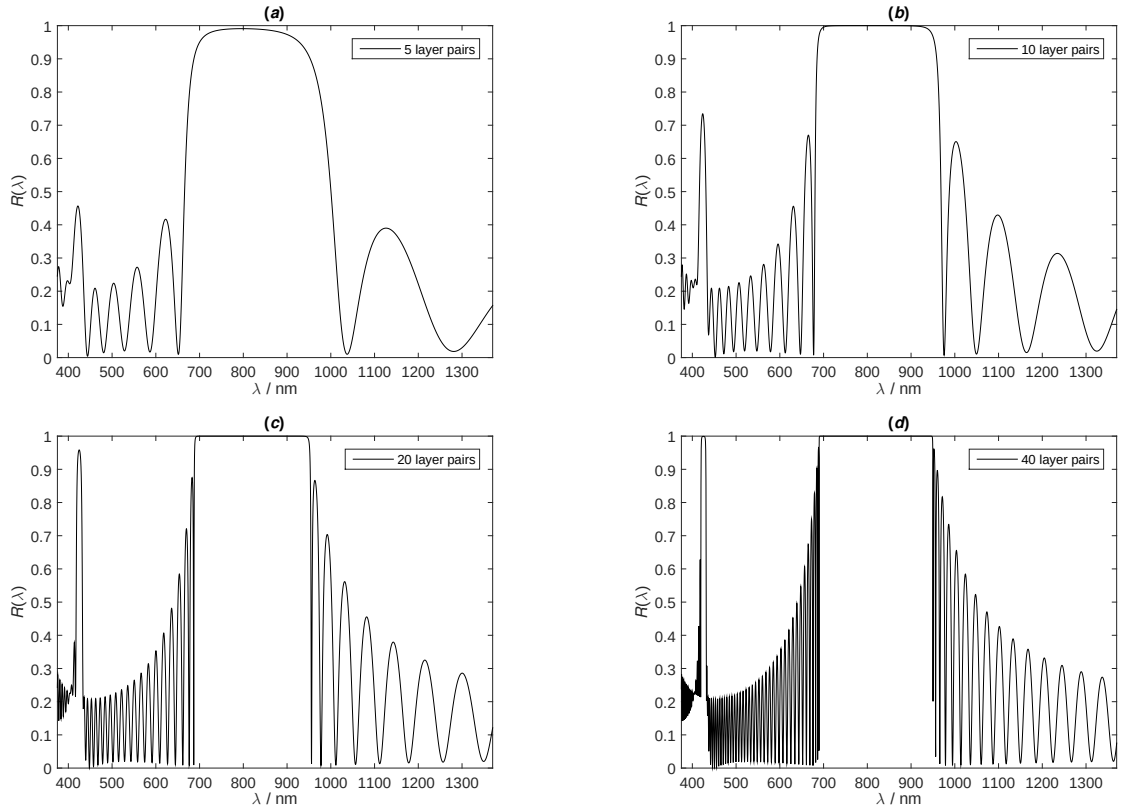

Figure 8: *(a)-(d) shows power reflectance as function of wavelength for Bragg mirrors with TiO_2 as substrate and outer layer. Note the "stop band" centered around 800 nm.*

The effect of an input pulse bandwidth exceeding the stop band also manifests itself in the time domain. Inside the stop band the GD is essentially constant at about 2-3 fs as shown in figure 9d. Therefore a pulse with most frequency components between 700 and 950 nm is simply delayed by this amount and is barely broadened nor chirped in any way. This is the case for the 20 fs pulse in figure 9a. A GD of a couple of femtoseconds means that the accumulated phase is on the order of 10 radians, equivalent to a penetration depth of only a few layers. Outside the stop band the situation is different. Here the GD is much higher in average and shows strong, irregular oscillations with wavelength. This implies the presence of high-order dispersion. The inevitable consequence for a pulse with a bandwidth broad enough to lose a part of its frequency content is thus an uneven smearing and delay in the time domain. This is visible in figure 9b and even more clearly seen in figure 9c for the 5 fs-pulse. The problem can be somewhat reduced by decreasing the number of layers, but that simultaneously lowers the reflectance.

The conclusion is thus that ordinary Bragg mirrors are unsuitable for reflecting sub-10 fs pulses for two reasons. Firstly, the pulse bandwidth exceeds the width of the stop band, limiting the reflectance and so defeats the purpose of using a dielectric mirror. Secondly, the strongly varying GD outside the stop band along with the missing frequencies temporally distorts and widens the pulse. These undesired effects worsen with decreasing τ.

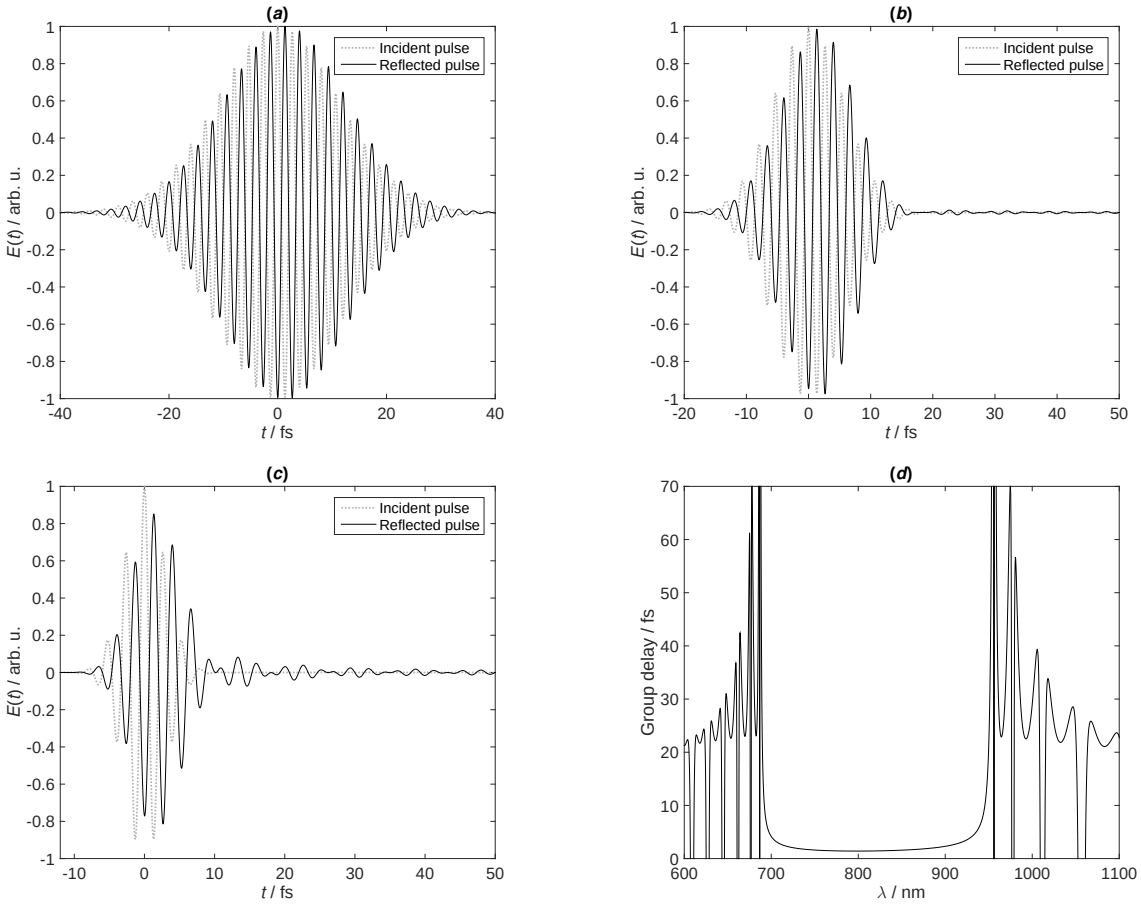

Figure 9: *(a)-(c) shows the real electric field in the time domain for incident pulses of duration 20, 10 and 5 fs respectively. This is for a TiO_2-substrate mirror with 20 layer pairs. (d) shows how the GD varies with wavelength for the same mirror.*

4.2 The linearly chirped mirror

Introducing a chirped mirror is primarily for the purpose of increasing the width of the stop band and to induce a controlled GDD in the pulse. A TiO_2-substrate mirror was selected to be the basis for this design since such mirrors performed best as simple Bragg reflectors studied in the previous section. Table 3 shows the reflectance parameters for such a mirror of linear chirp that has an increasing Bragg wavelength with mirror depth. Longer wavelengths are then maximally reflected deeper in the mirror, which should produce a negatively chirped pulse due to the anomalous dispersion. The table data is shown on the same format used in table 1 and 2. Each column contains results for a given range of the mirror chirp. Four different ranges were investigated because the chosen range would probably have a large impact on the mirror performance. For example, the leftmost column displays results where the outermost layer pair is optimized for reflection of 700 nm light, while the innermost pair is optimized for 1000 nm. The 5 fs input pulse was always used.

Table 3: *Power reflectance coefficient R_{tot} / ratio of peak intensities R_{max} for the different input pulses and chirped mirrors with TiO_2 as substrate and outermost layer.*

Number of layer pairs	Wavelength range spanned by layer chirp / nm			
	700 - 1000	550 - 1100	650 - 1250	600 - 1200
5	0.91281 / 0.70113	0.83760 / 0.39587	0.83455 / 0.65979	0.83923 / 0.56224
10	0.98016 / 0.66358	0.96438 / 0.31048	0.96147 / 0.58438	0.96439 / 0.39249
20	0.99432 / 0.63462	0.99868 / 0.23744	0.99632 / 0.50899	0.99841 /0.32793
40	0.99725 / 0.61959	0.99981 / 0.19447	0.99963/ 0.47514	0.99995 / 0.30993

It is immediately apparent that R_{tot} is greatly improved upon from the simple Bragg mirror, regardless of the wavelength range targeted by the chirp. There are some differences, however. For a small amount of layers it appears to be most efficient to concentrate on the central pulse wavelengths. This changes rapidly so that for 20 layer pairs it seems favorable to focus on the shorter wavelengths. For 40 pairs the design based on encompassing the entire pulse bandwidth is by far the best in terms of R_{tot}.

All designs appear to smear the pulse badly in the time domain since $R_{max} \ll 1$ in all cases. Targeting short wavelengths maximally smears the pulse, while chirping only for central wavelengths maintains the initial I_{max} fairly well. It must be stressed that a low R_{max} is not necessarily bad for a chirped mirror, though. Dispersion of some kind is expected, and an initially transform limited pulse affected by dispersion will inevitably widen temporally. What is important is rather that the GD varies consistently across the pulse bandwidth, so that only certain orders of dispersion are introduced in the pulse. It is namely much easier to compensate for dispersion if it is relatively uncomplicated.

In figure 10 the temporal effects of the design with 20 layer pairs and chirp range of 550-1100 nm are illustrated (a) together with the reflectance (b) and GD characteristics (c). As suggested by table 3, the stop band is very wide indeed. E_{max} (and thereby I_{max}) is low for the reflected pulse compared to the incident, and the pulse is widened by a great amount by the mirror. There is some negative chirp, but the irregular pulse shape implies many different higher orders of dispersion as well. Consequently, the difficulty of making the pulse transform limited again by dispersion compensation is immensely high. Designing an optical component with the complicated $\varphi(\lambda)$-characteristics required would be a nearly hopeless task.

The periodic oscillations in the GD as shown in figure 10c explain the irregular pulse shape in the time domain. Very similar oscillations are seen in figure 3.7 in Ref. [19] where a linearly chirped mirror is modelled. The cause of the oscillations appear to be interference between reflections in shallow and deep parts of the mirror, like in a so-called Gires-Tournois interferometer (GTI). The oscillations were first observed in 1985 [20] and not studied in detail as GTI-like effects until in 1999 [19]. To conclude: the naive expectation of a GD varying linearly with the wavelength is wrong and the simple chirped mirror would be useless inside a Ti:sapphire laser cavity or in an external pulse-shaping setup.

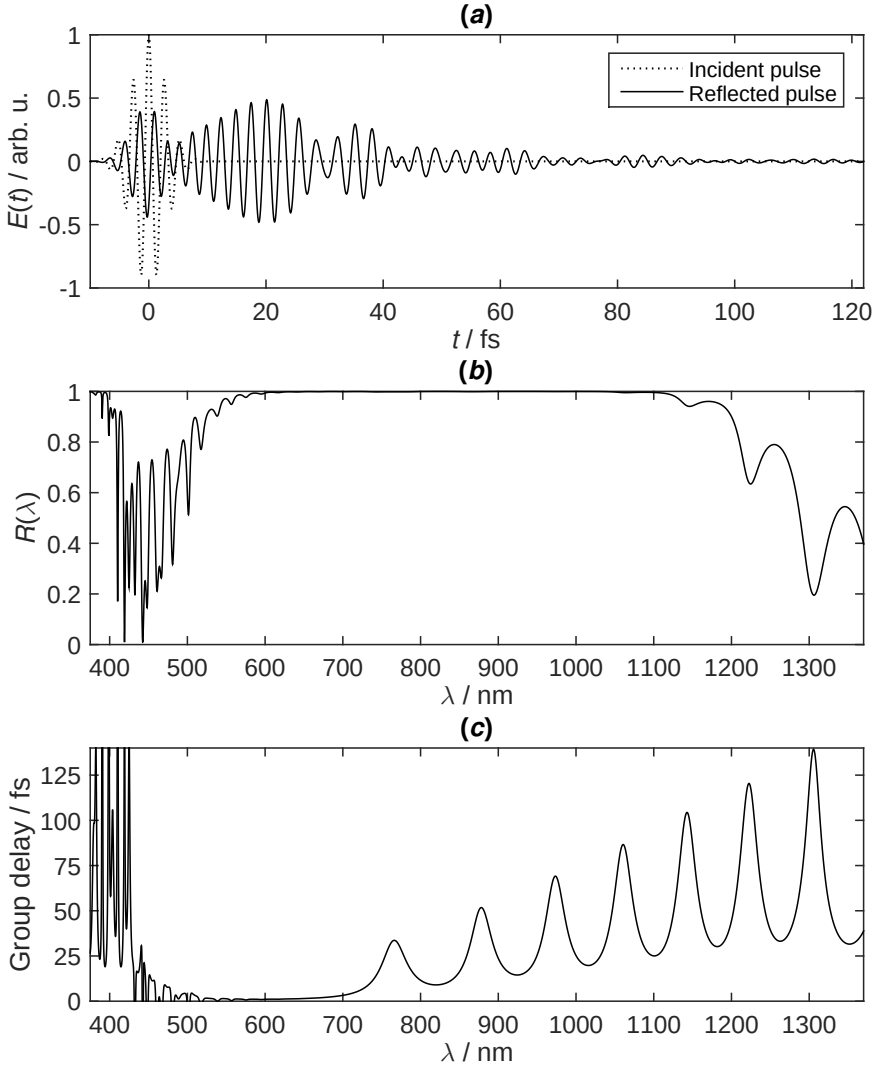

Figure 10: *Characteristics of a linearly chirped mirror with 20 layer pairs targeting 550 - 1100 nm. (a) Pulse shapes in the time domain for a 5 fs pulse. (b) Power reflectance: note the very wide stop band. (c) Group delay: note the oscillations.*

For completeness it must be said that the other mirror designs represented in table 3 result in plots very similar to those in figure 10. Especially noteworthy is that the main features of the GD oscillations are always the same, even though the position of the peaks and troughs varies between designs. This of course results in a somewhat different temporal pulse shape for every design. The general trend of the GD is however the desired linear increase with wavelength, which manifests itself as an overall slightly negative frequency chirp in $E(t)$.

If the mirror chirp could be somewhat modified, it would perhaps be possible to eliminate most of the oscillations so that only the linear trend remains. It is nevertheless not obvious at all at this stage how the design should deviate from the linear case presented here.

4.3 Accuracy of the simulations

What matters in the end is of course that actual fabricated dielectric mirrors exhibit the desired reflection properties demonstrated in section 4.1 and 4.2. The easiest way to investigate the accuracy of the TMM-based model in this thesis would of course be to manufacture one of the simulated designs using one of the techniques mentioned in section 2.6.3. Unfortunately this was beyond the scope of the thesis work. Models similar to this one are used by many research groups to simulate multilayers, though, and very often the obtained results seem to be in good agreement with experimental realizations. This is shown for example by figure 4 in Ref. [21]. Using a model which incorporates the bulk parameter that is the refractive index therefore appears to work well even if each mirror layer is only a couple of hundred atoms thick. It must be noted that the agreement with fabricated mirrors depend a lot on the manufacturing process. The refractive index can vary greatly with for example the pressure and temperature used.

The precision of the specific numerical model used here remains to be assessed. One of its advantages is that it takes into account the frequency dependence of n, thereby modelling the reflectivity and phase for every single frequency component more accurately compared to models which do not. Especially TiO_2 exhibits significant dispersion within the relevant wavelength range of 375-1370 nm, and so the benefit of using a unique n for every wavelength in the pulse is likely to be substantial. The advantage is strengthened further by the very detailed knowledge of the refractive indices across these wavelengths as is demonstrated in figure 7.

Applying r obtained by the TMM only for wavelengths between 375 and 1370 nm is likely to have a negative effect on the end results. Even the 20 fs pulse does after all contain spectral components outside this range. The amplitudes of these components are, however, very insignificant. At 375 nm the 5 fs pulse has a spectral intensity I_0 below a billionth of $I_{max} = I_0(\lambda_0)$ where $\lambda_0 = 800$ nm. At the other end of the spectrum at 1370 nm the situation is somewhat worse: I_0 for the 5 fs pulse is $1/2000$ of I_{max}, while the 10 and 20 fs pulses have values of I_0 below a billionth of I_{max}. The results for the 5 fs pulse are probably not notably affected by this though: $I_{max}/2000$ is still very insignificant. The wavelength range used is thus concluded to be wide enough to provide a very high accuracy for all pulses modelled here. If considering even shorter pulses than in this thesis, it would however be desirable to have access to refractive index data beyond 1370 nm.

When transforming back and forth between the time and frequency domain as done in this model it is important to have both a high temporal and spectral resolution. This is achieved by having a high sampling rate (or equivalently, a short sampling interval) and a time vector much longer than the pulses themselves. In the MATLAB-code used in the simulations a total of two million samples were used, spanning from -5000 to +5000 fs resulting in a sampling interval of 5 as. Since GD(λ) never goes higher than about 150 fs for any of the mirror designs, there should be virtually no observable aliasing effects in the time domain. This means that there is no noticeable "false signal" due to the periodicity

of the time vector. If the time vector would have been shorter than 150 fs, frequencies delayed by more than this amount would instead have appeared as such false signals in the other end of the time vector.

The conclusion is that the TMM-based method used in this thesis produces accurate results. Optical characteristics exhibited by one of the studied mirror designs manufactured with a high-precision technique should thus agree well with the simulations. The method is also very efficient: it takes only between ten and thirty seconds to run a simulation.

5 Summary and outlook

In this thesis, we have shown that if a Ti:sapphire laser is to be used for generation of 20 fs pulses or longer, ordinary Bragg mirrors can be used in the setup since they provide the necessary bandwidth with very high reflectance and an approximately constant GD. Bragg reflectors can for the same reasons also replace conventional mirrors outside the laser itself to guide the pulse along a desired beam path, with hardly any pulse energy loss or induced group delay variations. For shorter pulse durations a Bragg mirror fails to fulfill these two criteria as has been discussed in section 4.1.

Also shown in the thesis is that the linearly chirped mirror is a double-edged sword. It does exhibit an outstandingly wide stop band resulting in excellent reflectance for even a 5 fs pulse, but its unsatisfactory dispersion profile renders it useless. However, as implied in section 4.2 the tendency of the GD to increase linearly with wavelength is of key interest. A refinement of the linear chirp design might display only the linear variation, inducing a negative chirp in the reflected pulse. The normal dispersion exhibited by the Ti:sapphire crystal can then be compensated for, if the dispersion provided by the mirror is of the same magnitude as that of the crystal. The standard approach is to use a pair of prisms for dispersion compensation in a Ti:sapphire laser [8]. Since it imposes a negative GDD, a chirped mirror could replace the prism pair as the down-chirping optical component in the laser. Such mirrors have been devised via computer optimization, using a linearly chirped mirror like the one studied in section 4.2 as a starting design [22]. Replacing the prism pair would be greatly desired since the prisms exhibit substantial amounts of unwanted higher order dispersion which will notably affect very short pulses[6]. A correctly designed mirror, however, does not.

The solution to the GD oscillation problem is to have an anti-reflection coating on top of the mirror structure together with a slight additional chirp in layer thickness, affecting how strongly a wave incident on a given layer interferes with the wave reflected off of that layer. This is called a *double-chirped mirror*. How such a mirror has to be chirped to achieve a certain desired GD(λ)-curve can been derived analytically [23]: the important result is often called the *chirp law*. This law is not exact: mirror designs based on the

[6] See figure 3.3 in Ref. [19]

chirp law still have to be fine-tuned using numerical optimization. GD(λ) for a given starting design determined by the chirp law does not, however, deviate very much from the desired dispersion characteristics.

The analytical description of chirped mirrors has resulted in rapid progress: double-chirped mirrors with dispersion curves based on the chirp law are now commercially available and used in many femtosecond laser systems. New areas of applications for such dielectric mirrors have also started to appear as a result of recent advances in attosecond science. The pulses generated in the HHG process are often chirped and consequently not as short as a transform limited pulse of the same frequency content. A chirped mirror with the opposite GDD of the pulse itself could thus be used to bring the frequency components together in time, shortening the pulse durations. This has been done theoretically as reported in a recent paper [24]. These promising results indicate that the already short pulses could potentially be compressed down to durations of only tens of attoseconds.

It was stated in section 2.5 that methods based on the transfer matrix method could ”be used to model propagation through any kind of multilayer optics”. The results obtained for the mirror designs in section 4 support this claim, and this is further validated for instance by ref. [25], where a multilayer mirror reflecting an attosecond pulse is modelled employing a transfer matrix approach combined with FFT. This clearly demonstrates the applicability and generality of the main analysis framework used in this thesis, which thus should provide a basis for further studies in the field of ultrafast optics.

Acknowledgements

I would like to thank my supervisor, Per Johnsson, for introducing me to the exciting research field of ultrafast science and for the support he has given me during the thesis work.

Thanks should also go to my classmate Thomas Kjellberg Jensen for the very fruitful discussions we have had during the writing of our theses.

Last but not least: many thanks to the coffeemaker in ”Rydbergs källare” at Fysicum for its never-ending supply of liquid productivity.

References

[1] C. V. Shank and E. P. Ippen. Subpicosecond kilowatt pulses from a mode-locked cw dye laser. *Applied Physics Letters*, 24(8):373–375, 1974. doi:10.1063/1.1655222.

[2] U. Morgner, F. X. Kärtner, S. H. Cho, Y. Chen, H. A. Haus, J. G. Fujimoto, E. P. Ippen, V. Scheuer, G. Angelow, and T. Tschudi. Sub-two-cycle pulses from a Kerr-lens mode-locked Ti:sapphire laser. *Optics letters*, 24(6):411–413, 1999. doi:10.1364/OL.24.000920.

[3] Ahmed H. Zewail. Femtochemistry. Past, present, and future. *Pure and Applied Chemistry*, 72(12):2219–2231, 2000. doi:10.1351/pac200072122219.

[4] Anne L'Huillier, M. Lewenstein, P. Salières, Ph. Balcou, M. Yu Ivanov, J. Larsson, and C. G. Wahlström. High-order Harmonic-generation cutoff. *Physical Review A*, 48(5):69–72, 1993. doi:10.1103/PhysRevA.48.R3433.

[5] C. G. Wahlström, J. Larsson, A. Persson, T. Starczewski, S. Svanberg, P. Salières, Ph. Balcou, and Anne L'Huillier. High-order harmonic generation in rare gases with an intense short-pulse laser. *Physical Review A*, 48(6):4709–4720, 1993. doi:10.1103/PhysRevA.48.4709.

[6] P. Johnsson. *Attosecond Optical and Electronic Wave Packets*. PhD thesis, Lund University, 2006.

[7] Pierre Agostini and Louis F. DiMauro. The physics of attosecond light pulses. *Reports on Progress in Physics*, 67(8):1563–1563, 2004. doi:10.1088/0034-4885/67/8/C01.

[8] J. Zhou, G. Taft, C. P. Huang, M. M. Murnane, H. C. Kapteyn, and I. P. Christov. Pulse evolution in a broad-bandwidth Ti:sapphire laser. *Optics letters*, 19(15):1149–1151, 1994. doi:10.1364/OL.19.001149.

[9] B.E.A. Saleh and M.C. Teich. *Fundamentals of Photonics*. John Wiley & Sons, Inc., 2nd edition, 2007.

[10] John David Jackson. *Classical Electrodynamics*. John Wiley & Sons, Inc., 3rd edition, 1999.

[11] M. N. Polyanskiy. Refractive Index database. Visited 2015-03-05. URL: http://refractiveindex.info.

[12] R. Redheffer. Difference equations and functional equations in transmission-line theory. In *Modern Mathematics for the Engineer*, chapter 12. McGraw-Hill, New York, 1961.

[13] R. Paschotta. Metal-coated mirrors, *Encyclopedia of Laser Physics and Technology*. Visited 2015-04-06. URL: http://www.rp-photonics.com/metal_coated_mirrors.htm.

[14] R. Paschotta. Dielectric Coatings, *Encyclopedia of Laser Physics and Technology*. Visited 2015-04-06. URL: http://www.rp-photonics.com/encyclopedia_cite.html?article=dielectriccoatings.

[15] I. H. Malitson. Interspecimen Comparison of the Refractive Index of Fused Silica. *Journal of the Optical Society of America*, 55(10):1205, 1965. doi:10.1364/JOSA.55.001205.

[16] J. R. Devore. Refractive Indices of Rutile and Sphalerite. *Journal of the Optical Society of America*, 41(6):416, 1951. doi:10.1364/JOSA.41.000416.

[17] Refractive Index of SiO2, *Filmetrics, Inc.* Visited 2015-03-12. URL: http://www.filmetrics.com/refractive-index-database/SiO2/Fused-Silica-Silica-Silicon-Dioxide-Thermal-Oxide-ThermalOxide.

[18] Refractive Index of TiO2, *Filmetrics, Inc.* Visited 2015-03-12. URL: http://www.filmetrics.com/refractive-index-database/TiO2+-+Amorphous/Titanium-Dioxide.

[19] Nicolai Matuschek. *Theory and Design of Double-Chirped Mirrors*. PhD thesis, Swiss Federal Institute of Technology Zürich, 1999.

[20] P. Laporta and V. Magni. Dispersive effects in the reflection of femtosecond optical pulses from broadband dielectric mirrors. *Applied optics*, 24(13):2014, 1985. doi:10.1364/AO.24.002014.

[21] F.X. Kärtner, N. Matuschek, T. Schibli, U. Keller, H.A. Haus, C. Heine, R. Morf, V. Scheuer, M. Tilsch, and T. Tschudi. Design and fabrication of double-chirped mirrors. *Optics letters*, 22(11):831–833, 1997. doi:10.1364/OL.22.000831.

[22] R. Szipocs, K. Ferencz, C. Spielmann, and F. Krausz. Chirped multilayer coatings for broadband dispersion control in femtosecond lasers. *Optics letters*, 19(3):201, 1994. doi:10.1364/OL.19.000201.

[23] Nicolai Matuschek, Franz X. Kärtner, and Ursula Keller. Analytical Design of Double-Chirped Mirrors with Custom-Tailored Dispersion Characteristics. *IEEE Journal of Quantum Electronics*, 35(2):129–137, 1999. doi:10.1109/3.740733.

[24] Alexander Guggenmos. Aperiodic multilayer mirrors for attosecond soft x-ray pulses. *SPIE Optical ...*, 8502(400 mm):1–7, 2012. URL: http://proceedings.spiedigitallibrary.org/proceeding.aspx?articleid=1382033, doi:10.1117/12.930762.

[25] Cheng-You Lin and Da-He Liu. Reflecting a single attosecond pulse by using periodic Mo/Si multilayer mirrors with different layers. *Chinese Physics B*, 21(9):094216, 2012. doi:10.1088/1674-1056/21/9/094216.